AIMS Materials Science, 4(2): 487-502.
DOI: 10.3934/matersci.2017.2.487
Received: 31 January 2017
Accepted: 17 March 2017
Published: 22 March 2017

http://www.aimspress.com/journal/Materials

Research article

A facile microwave approach to synthesize RGO-$BaWO_4$ composites for high performance visible light induced photocatalytic degradation of dyes

Mohamed Jaffer Sadiq Mohamed and Denthaje Krishna Bhat *

Department of Chemistry, National Institute of Technology Karnataka, Surathkal, Mangalore-575025, Karnataka, India

* **Correspondence:** Email: denthajekb@gmail.com.

Abstract: Photocatalysts with enhanced efficiency for environmental remediation requires an effective separation of photogenerated electron hole pairs and optimum charge carrier transport. Based on the above criteria, a cost effective, facile one-pot microwave approach was made to synthesize RGO-$BaWO_4$ composites with excellent stability and reusability in photodegradation of methylene blue (MB) and methyl orange (MO). A series of composites with varying composition with respect to RGO was synthesized and thoroughly characterized using various techniques. The composite with 2.5% RGO-$BaWO_4$ showed maximum efficiency under visible light irradiation. The mechanism of charge transfer and kinetics of the reaction was also studied. The interfacial/interparticle charge transfer between the narrow elliptical $BaWO_4$ particles and RGO is found to be responsible for the increased efficiency. The photo generated holes and the superoxide radical were found to play a key role in the degradation process. The synergistic action makes RGO-$BaWO_4$ composites a promising material as high performance photocatalyst for degradation of organic dyes.

Keywords: RGO-$BaWO_4$ composites; microwave method; photodegradation; methylene blue; methyl orange

1. Introduction

The wastes discharged from various industries and plants are the major source of water pollution, ringing alarm bells for human society. Organic dyes are mainly used in industries related to textile, cosmetics, paper, pharmaceuticals, food, printing and dyeing. Around 20% of these dyes are lost during the process of coloring. Since these are lost into the water their removal from the water sources has become a major environmental issue [1,2]. For the treatment of hazardous wastes, several conventional methods like reverse osmosis, adsorption, ultra filtration, coagulation by chemical agents, enzymes, etc, are used [3–7]. But these nondestructive processes just transfer the pollutants from one phase to another, creating secondary pollutants. Hence for mineralization of the organic dyes with aromatic moieties, an eco-friendly cost effective method has to be implemented in large scale. Photocatalysis is one such process which has been looked into for a past couple of decades, but the high recombination rate of photo generated electrons and holes has prevented it from commercialization of the application [8,9,10].

Semiconducting materials with narrow band gap have been used as photocatalyst since the band gap energy corresponds to the UV or visible light region of the solar spectrum and also they help in charge separation. Materials like TiO_2, ZnO, Fe_2O_3, NiO, Co_3O_4, CeO_2, ZrO_2 have tunable physical and optical properties [11–16]. Among these, TiO_2 is a well-known photocatalyst with high chemical stability, non toxicity, photo corrosion resistivity and low cost. But it suffers from the disadvantage of having a wide band gap of 3.2 eV which leads to absorption of only a very small portion of the solar energy and has a higher recombination rate of electron-hole pairs. Multi metal oxides like $SrTiO_3$, $LaFeO_3$, $NaTaO_3$, $BaFeO_3$, $K_4Nb_6O_{17}$, $CaIn_2O_4$, $CaBi_2O_4$ and $BiVO_4$ have also been used for photodegradation of organic pollutants [15,17]. Of late $M^{2+}WO_4$ type metal tungstates is under the research radar and nano/micro structured materials like $CdWO_4$, $ZnWO_4$ and $NiWO_4$ have been applied in variety of areas [1,15,18,19].

$BaWO_4$ which has a wide variety of applications in the field of lasers, catalysis, scintillators, fluorescent lamps, photoluminescence and optical fibers, have been studied very less in the field of photocatalysis [20]. Although several methods of preparation have been reported for this material such as Czochralski, precipitation, hydrothermal, solid state and pulsed laser deposition the material still suffered instability and slow electron transfer rate. Since visible region of the solar spectrum is more dominant, $BaWO_4$ which is a UV catalyst has to be transformed to visible light absorbing entity to make it more applicable [20]. For visible light absorption the band gap has to be small which means the recombination rate will be very high. By doping carbon containing species the transport property and the recombination rate can be altered desirably to improve the photocatalytic efficiency [1,18,19].

Graphene known to be mother of all 2D materials has excellent properties [21,22]. Reduced graphene oxide (RGO) can be prepared from graphene oxide (GO) via Hummer's and modified Hummer's method during which metal and metal oxides can be added to decorate the nanosheets [23,24]. RGO can act as a support system in the composite while also retaining the photogenerated electron thus reducing the recombination rate of electron-hole pair; it improves the adsorption of the dye molecules via π–π interaction. Several RGO based nanocomposites have been reported for photocatalytic applications but to the best of our knowledge RGO-$BaWO_4$ composites have not yet been studied for their photocatalytic performance [24].

Microwave approach of synthesis has an upper hand over the conventional thermal synthesis due to the factors like microwave irradiation directly heats the material rather than heating the reaction vessel and hence consumes less energy and time; uniform heating; selective heating; acceleration in reaction rate and high chemical yield. Recently, microwave approach has been used to synthesize RGO, metal tungstates and RGO hybrid composites for application in the field of photocatalysis, hydrogen generation and supercapacitors [21,25,26].

In view of the aforesaid facts, we thought it is worthwhile to synthesize RGO-$BaWO_4$ composites of varied compositions using microwave approach. The as synthesized materials were characterized using X-ray diffraction (XRD), Scanning electron microscopy (SEM), Energy dispersive X-ray (EDX) analysis, X-ray photoelectron spectroscopy (XPS), Raman spectroscopy to determine the phase structure, morphology and elemental composition. Photoluminescence spectroscopy (PL) and Diffuse reflectance spectroscopy (DRS) techniques were used to study their optical properties. The photocatalytic activity was studied through photodegradation of methylene blue (MB) and methyl orange (MO) dyes under visible light. The stability and reusability of the composites were also determined. A reaction mechanism was proposed based on active species trapping experiment to determine the species involved in photocatalytic degradation of dyes.

2. Materials and Method

2.1. Materials

All the reagents procured were of analytical grade and utilized without further purification. Deionized water was utilized for all the experiments.

2.2. Synthesis of GO

GO was synthesized as reported earlier using modified Hummer's method [27,28]. The typical procedure is as follows: graphite flakes (about 1 g) was mixed well with $KMnO_4$ (about 4 g). To this conc. sulphuric acid (90 mL) was added slowly in about 30 minutes under magnetic stirring. The mixture was further stirred for 12 h after which deionized water (80 mL) and hydrogen peroxide (30%) were added till the color changed from greenish purple to bright yellow. This suspension was centrifuged and the supernatant was decanted. The precipitate was washed with water and hydrochloric acid (10%). It was vacuum dried at 60 °C for 12 h.

2.3. Synthesis of RGO-$BaWO_4$ Composites

In a typical experiment, $Ba(CH_3COO)_2$ and $Na_2WO_4{\cdot}2H_2O$ each was dissolved in 20 mL mixture of ethylene glycol and water (1:1) under magnetic stirring for about 20 minutes at room temperature. 0.005 M solutions (20 mL each) of both were mixed to which calculated amounts of exfoliated GO was added and stirred for 30 minutes to prepare a series of xRGO-$BaWO_4$ composites where x = 0, 1, 2.5, 5 and 10. The exfoliation of GO was done by ultrasonicating the GO solution for 30 minutes. The solution containing GO, $Ba(CH_3COO)_2$ and $Na_2WO_4{\cdot}2H_2O$ was then taken into a 100 mL reactor and irradiated with microwave of 350 W for 2 minutes. After the solution cooled down naturally the precipitate was collected by centrifuging. It was washed with water and ethanol

(10%) several times and vacuum dried at 60 °C for 12 h. The prepared samples were denoted as 1% RGO-$BaWO_4$, 2.5% RGO-$BaWO_4$, 5% RGO-$BaWO_4$ and 10% RGO-$BaWO_4$, respectively, with the number referring to the weight ratios of RGO to $BaWO_4$. A control sample of $BaWO_4$ was synthesized using a similar process without addition of GO.

2.4. Characterization

The crystal structures of RGO-$BaWO_4$ composites were determined by XRD (X-6000, Shimadzu) with Cu K_α radiation ($\lambda = 0.154$ nm). The morphologies of the composites were examined with a SEM (JEOL JSE-6390) well equipped with EDX operated at a voltage of 15.0 kV. The elemental composition of the composites was determined using XPS (XPS, Kratos XSAM800) equipped with standard and monochromatic X-ray sources (Al-Kα). Raman spectra were obtained by Horiba Jobin Yvon, Japan at room temperature using a 532 nm laser as radiation source. DRS of the composites were recorded by utilizing UV-visible spectrometer (Analytik Jena). The room temperature PL spectra of the composites were obtained by using a Horiba Jobin Yvon PL instrument. The specific surface area of the samples was measured on SMART SORB 92/93 (Smart Instruments Company Private Limited, INDIA) using Brunauer-Emmett-Teller (BET) method.

2.5. Photocatalytic Measurements

The photocatalytic performance of the RGO-$BaWO_4$ composites was determined in visible light region by the degradation of MB and MO solution. A pyrex glass photocatalytic reactor furnished with water cooled immersion tube, 250 W Hg lamp (emission range from 300 to 800 nm), cut-off filter of wavelength 400 nm and sample extracting facility was utilized to illuminate the suspension (100 mL) containing the dye (10 mg/L) and the photocatalyst (0.1 g). The reaction mixture was maintained at a pH of 3 using 0.1 N H_2SO_4. The suspension was allowed to achieve adsorption-desorption equilibrium by stirring it for 30 minutes in dark. Once the solution is irradiated at regular intervals, 4 ml of the suspension is withdrawn. It is centrifuged and the supernatant is subjected to UV-visible analysis. The photodegradation efficiency was estimated according to the equation, degradation % = $[(C_0 - C)/C_0] \times 100$, where C_0 represents the initial concentration of the dye and C represents the concentration of the dye after irradiation at time interval "t".

3. Results and Discussion

3.1. X-ray Diffraction Analyses

The XRD patterns of graphite, GO, RGO, $BaWO_4$ and RGO-$BaWO_4$ composites with various RGO weight proportions are shown in Figure 1. The XRD pattern of GO revealed only one sharp peak. The diffraction peak (002) of GO is situated at $2\theta = 10.5°$ with d-spacing of about 0.842 nm. This value of d-spacing is larger than that of pristine graphite (0.339 nm) indicating the presence of intercalated oxygen containing functional groups [29]. The absence of peaks corresponding to graphite in GO pattern indicates that graphite has been completely oxidized to GO. The diffraction peaks corresponding to RGO-$BaWO_4$ composite can be indexed to scheelite type tetragonal crystal of $BaWO_4$ with space group I41/a indicating that incorporation of $BaWO_4$ into RGO matrix does not

change the crystal structure of the former. The diffraction peaks found at 2θ values 17.25°, 26.45°, 28.06°, 31.87°, 42.97°, 45.68°, 48.69°, 53.57°, 54.48°, 66.59°, 67.74°, 69.36°, 73.0°, 73.77°, 75.75° and 76.83° can be ascribed to (101), (112), (004), (200), (204), (220), (116), (312), (224), (400), (208), (411), (332), (404), (420) and (228) planes of $BaWO_4$ (JCPDS card no. 43-0646), respectively. The absence of impurity peaks indicated the high purity of the samples.

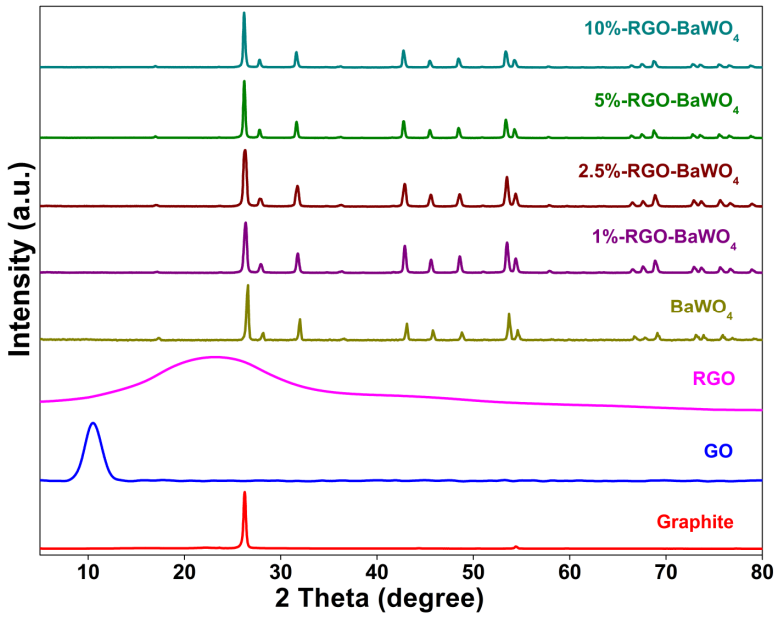

Figure 1. XRD patterns of the graphite, GO, RGO, $BaWO_4$ and RGO-$BaWO_4$ composites of different compositions.

3.2. SEM and EDX analyses

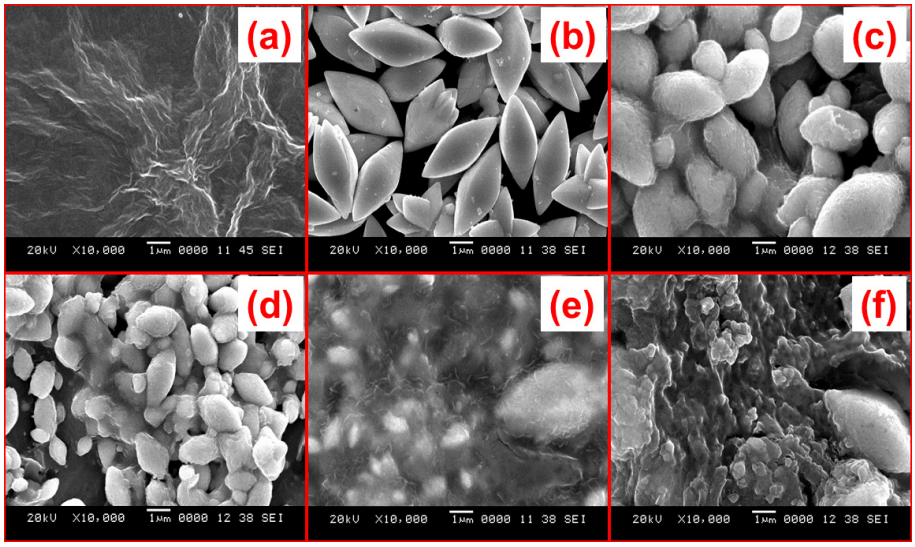

Figure 2. SEM images of (a) Pure RGO, (b) Pure $BaWO_4$, (c) 1% RGO-$BaWO_4$ composite, (d) 2.5% RGO-$BaWO_4$ composite, (e) 5% RGO-$BaWO_4$ composite, (f) 10% RGO-$BaWO_4$ composite.

The morphologies of the $BaWO_4$ and RGO-$BaWO_4$ composites were studied using SEM (Figure 2). The SEM image reveals narrow elliptical $BaWO_4$ particles. In the composite we notice the $BaWO_4$ particles wrapped in RGO sheets. The elemental composition was found to be C, Ba, W and O by EDX analyses (Figure 3). Ba, W and O were present in the ratio 1:1:4 indicating the presence of $BaWO_4$. Elemental mapping of C, Ba, W and O using spot EDX revealed uniform distribution of $BaWO_4$ in RGO matrix in RGO-$BaWO_4$ composites (Figure 3a–d).

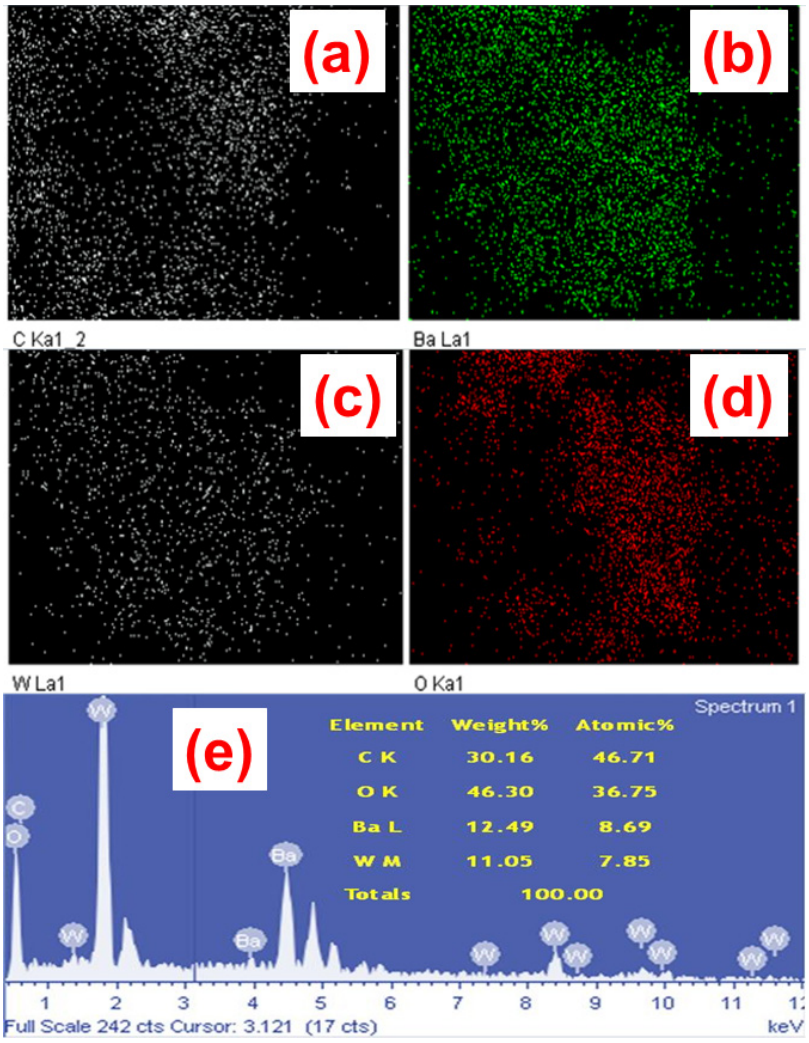

Figure 3. Spot EDX of (a) C; (b) Ba; (c) W; (d) O in the RGO-$BaWO_4$ composites; (e) EDX spectrum of RGO-$BaWO_4$ composites.

3.3. XPS Analyses

XPS is a highly sensitive surface technique used to determine the elemental composition, chemical and electronic state of the element within a material. The XPS survey spectrum (Figure 4a) of RGO-$BaWO_4$ composite exhibits peaks corresponding to C 1s, O 1s, Ba 3d and W 4f. The high resolution deconvoluted C 1s XPS spectra for GO (Figure 4b), reveals four peaks located at 284.6 eV, 285.8 eV, 286.9 eV and 288.7 eV which corresponds to the C–C (sp^2 bonded carbon), C–OH (hydroxyls), C=O (carbonyls) and O–C=O (carboxyl) functional groups, respectively indicating high

oxygen content on the surface [18]. High resolution deconvoluted C 1s spectrum of RGO-$BaWO_4$ (Figure 4c) reveals a peak around 284.6 eV, corresponding to C–C (sp^2 bonded carbon). The intensity of peaks corresponding to the oxygen functional groups decreased drastically indicating the reduction of GO into RGO successfully [19].

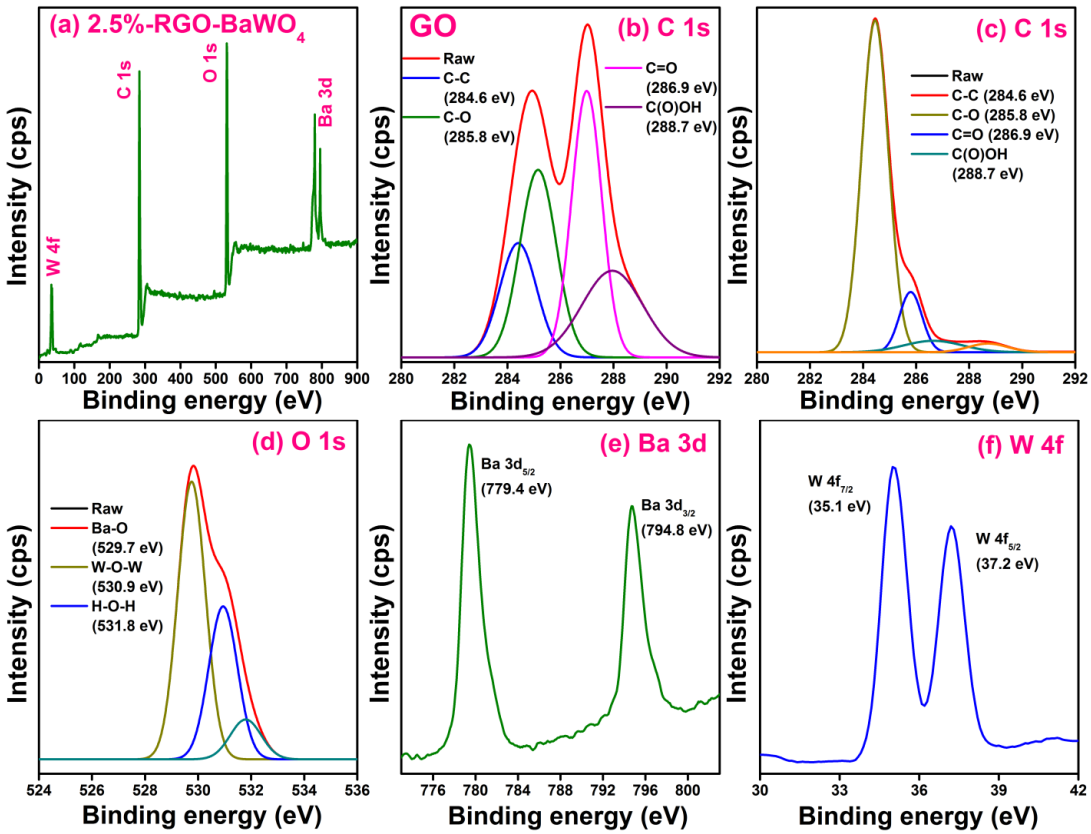

Figure 4. (a) XPS survey spectrum of the RGO-$BaWO_4$ composite; (b) XPS spectrum of GO C 1s; XPS spectrum of RGO-$BaWO_4$ composite (c) C 1s; (d) O 1s; (e) Ba 3d; (f) W 4f .

The high-resolution Ba 3d spectrum (Figure 4d) comprises of two peaks at 779.4 eV and 794.8 eV, corresponding to Ba $3d_{5/2}$ and Ba $3d_{3/2}$, respectively. The high-resolution W 4f spectrum (Figure 4e) also comprises of two peaks at 35.1 eV and 37.2 eV, which corresponds to the W $4f_{7/2}$ and W $4f_{5/2}$, respectively. The splitting energy between the 4f doublet of W is 2.1 eV indicates that W is in +6 state [19]. The high-resolution O 1s spectrum (Figure 4f) consists three peaks at 529.7 eV, 530.9 eV and 531.8 eV, which corresponds to the Ba–O, W–O–W and H–O–H (surface absorbed hydroxyl oxygen species), respectively [1,18].

3.4. Raman Analyses

Raman spectroscopy is a fast and nondestructive technique to obtain vibrational information about the chemical bonds and symmetry of the molecule. The Raman spectra for GO, RGO, $BaWO_4$, and RGO-$BaWO_4$ composite are shown in Figure 5. The Raman spectra of GO reveals two

prominent peaks at around 1346.4 cm^{-1} and 1598.1 cm^{-1} corresponding to the D band (the breathing mode of the symmetry A_{1g}) and the G band (the E_{2g} mode of sp^2 carbon atoms), respectively [18,19]. $BaWO_4$ on the other hand exhibits three peaks around 333.6 cm^{-1}, 794.5 cm^{-1} and 927.1 cm^{-1}, which corresponds to the Raman active vibrations of A_g, B_g and E_g modes, where A and B are non-degenerate modes while E is doubly degenerate mode [30]. The subscript g refers to the centrosymmetric nature.

Two prominent D and G bands are exhibited around 1339.6 cm^{-1} and1594.8 cm^{-1} by RGO and around 1338.2 cm^{-1} and 1592.5 cm^{-1} by RGO-$BaWO_4$ composite, respectively. The 2D bands appear at 2653.2 cm^{-1} and 2639.1 cm^{-1} in the case of RGO and RGO-$BaWO_4$, respectively. The decrease in the wavenumbers of D and G bands from GO to RGO, indicates the conversion of GO to RGO [18,19]. The further decrease in the wavenumbers after the formation of the composite is due to the smaller size of $BaWO_4$ crystals.

The I_D/I_G intensity ratio of pure RGO and RGO in RGO-$BaWO_4$ composite (1.07 and 1.10, respectively) is slightly greater than that of GO (0.75). This is may be due to the decrease in the sp^2 domain size as GO gets reduced to RGO nanosheets [19]. The domain size can be calculated by using equation (1),

$$L = 4.4/(I_D/I_G) \quad (1)$$

where, L = domain size and I_D/I_G is the intensity ratio of D and G bands. The calculated domain size of GO, RGO and RGO-$BaWO_4$ are 5.87 nm, 4.11 nm and 4.0 nm, respectively.

The number of RGO layers can be determined by the ratio I_{2D}/I_G, where I_{2D} is intensity of 2D band and I_G is intensity of G band. The ratio I_{2D}/I_G of >2, 1 to 2, and <1 corresponds to single, double and multi-layer of RGO sheets, respectively. In the present work I_{2D}/I_G was found to be 0.34 and 0.42 for RGO and RGO-$BaWO_4$ composite, respectively indicating the multilayered nature of RGO sheets.

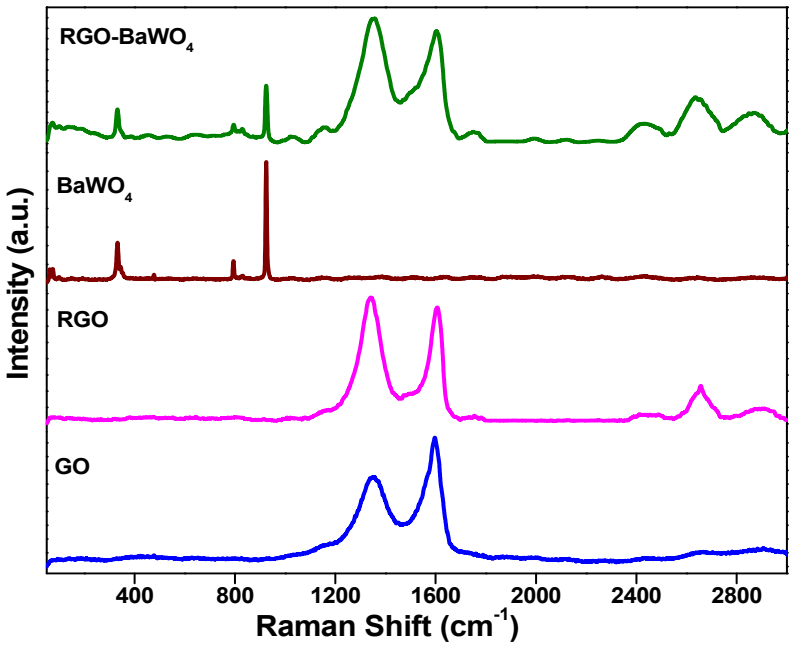

Figure 5. Raman spectra of the GO, RGO, $BaWO_4$ and RGO-$BaWO_4$ composites.

3.5. DRS Analyses

The optical properties of the as-synthesized composites were studied using DRS (Figure 6a). The results indicated that $BaWO_4$ absorbs in the UV region while the absorption edge of the RGO-$BaWO_4$ composites shifts towards the visible region with increase in the intensity of absorption. The DRS of pure RGO shows that although its absorption maximum occurs in the UV region it has sufficiently high absorbance in the visible region compared to that of pure $BaWO_4$. Thus, the observed red shift in the absorption edge of the composites may be due to the increasing amounts of RGO in the composites. The results also suggest that $BaWO_4$ is incapable of acting as a photocatalyst in the visible region while the composites can be active in the visible region as photocatalysts due to appropriate band gap.

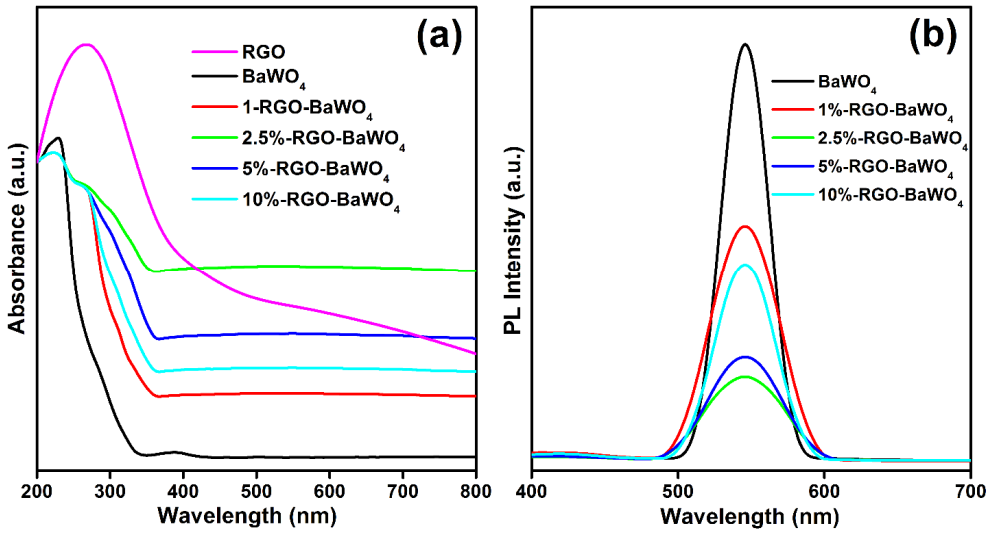

Figure 6. (a) DRS; (b) PL spectra of the $BaWO_4$ and RGO-$BaWO_4$ composites.

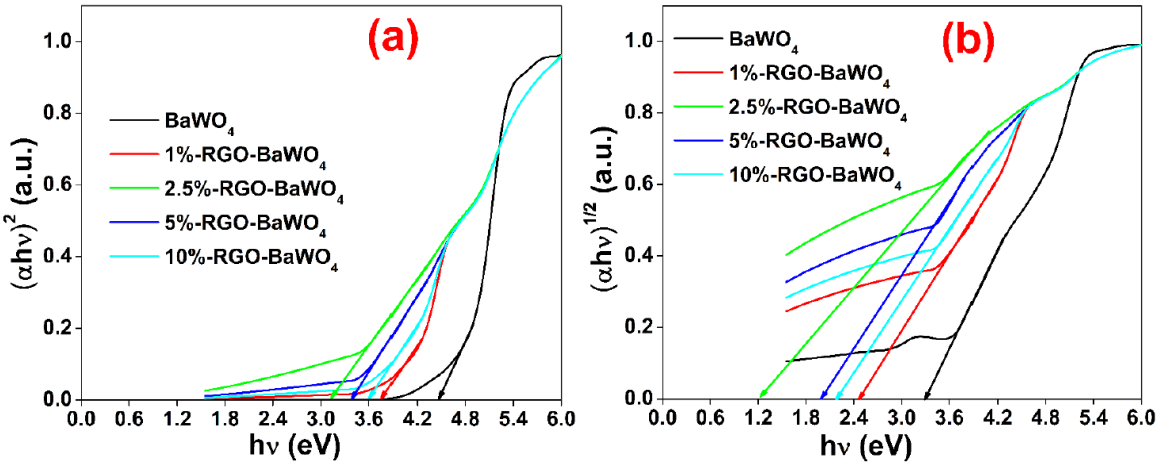

Figure 7. Band gap plots of $BaWO_4$ and RGO-$BaWO_4$ composites (a) direct; (b) indirect.

The band gap energy was calculated employing the Kubelka-Munk equation (2),

$$\alpha(h\nu) = A(h\nu - E_g)^{n/2} \quad (2)$$

where α, h, ν, E_g and A are the absorption coefficient, Plank constant, frequency of light, band gap energy and constant, respectively. The "n" value of 1 corresponds to direct and 4 corresponds to indirect transition in the semiconductor material. The band gap is determined by a plot of $(\alpha h\nu)^{n/2}$ versus energy of photon (hν). Direct band gap energy of 4.43 eV, 3.76 eV, 3.60 eV, 3.39 eV, 3.13 eV and indirect band gap energy of 3.30 eV, 2.47 eV, 2.19 eV, 1.99 eV, 1.22 eV corresponding to pure $BaWO_4$, 1% RGO-$BaWO_4$, 10% RGO-$BaWO_4$, 5% RGO-$BaWO_4$ and 2.5% RGO-$BaWO_4$ respectively (Figure 7). The values of direct and indirect band gaps indicate that the RGO-$BaWO_4$ composites respond to both UV as well as visible light.

3.6. PL Analyses

PL spectra can be used to determine the effectiveness of the charge separation and recombination rate of the photogenerated electron hole pairs. If the intensity of PL peak is lower it means the recombination rate is lower [1]. The PL spectra of the as-synthesized $BaWO_4$ composites with various amount of RGO are shown in Figure 6b. The excitation wavelength corresponds to 400 nm while the emission peak is exhibited around 545 nm (green emission). $BaWO_4$ shows highly intense peak indicating high recombination rate. The composites exhibit lower intensity than pure $BaWO_4$. 2.5% RGO-$BaWO_4$ shows very less intensity indicating the low recombination rate of electron hole pairs generated by the visible light irradiation.

3.7. Surface Area Analyses

The BET surface area analyses of the composite samples were carried out to study the effect of addition of RGO on the overall surface area of prepared nanocomposites. The measured BET surface areas of the samples were, 3.41 m^2/g, 14.14 m^2/g, 19.45 m^2/g, 18.95 m^2/g and 15.95 m^2/g for pure $BaWO_4$, 1% RGO-$BaWO_4$, 2.5% RGO-$BaWO_4$, 5% RGO-$BaWO_4$ and 10% RGO-$BaWO_4$ respectively. The addition of RGO content initially increased the surface area of the sample up to RGO content of 2.5%. Further additions of RGO did not increase the surface area. This may be due to agglomeration of RGO and $BaWO_4$ in the formed composite.

3.8. Photocatalytic Analyses

The photocatalytic degradation of MB and MO were studied in the presence of RGO-$BaWO_4$ in aqueous solution using visible light source. Degradation of dye (i) in presence of photocatalyst, in the absence of irradiation and (ii) in the absence of photocatalyst with visible light irradiation, were considered as control (blank test). Under visible light irradiation the color of the solution changed with time indicating the photodegradation was in progress. The absorption intensity decreased with time as shown in Figure 8.

The absorbance peaks of MB and MO appearing at 664 nm and 464 nm decreased with time and disappeared completely after 120 minutes and 165 minutes, respectively. The photodegradation efficiencies of various catalyst compositions were compared (Figure 9a–b) and it was found that both in the case of MB and MO dye degradation 2.5% RGO-$BaWO_4$ composite showed maximum efficiency.

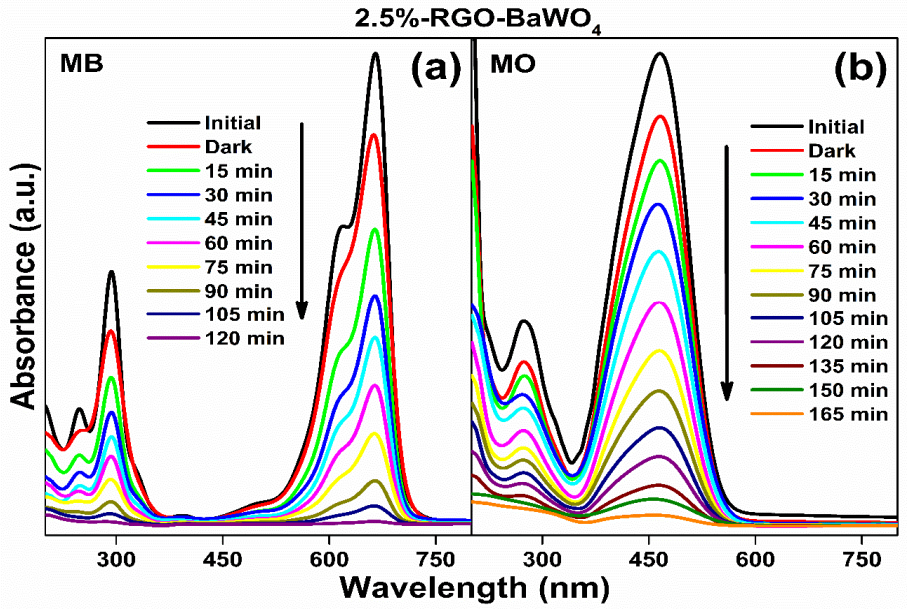

Figure 8. UV-Vis spectra of (a) MB; (b) MO concentration changes with time in the presence of 2.5% RGO-$BaWO_4$.

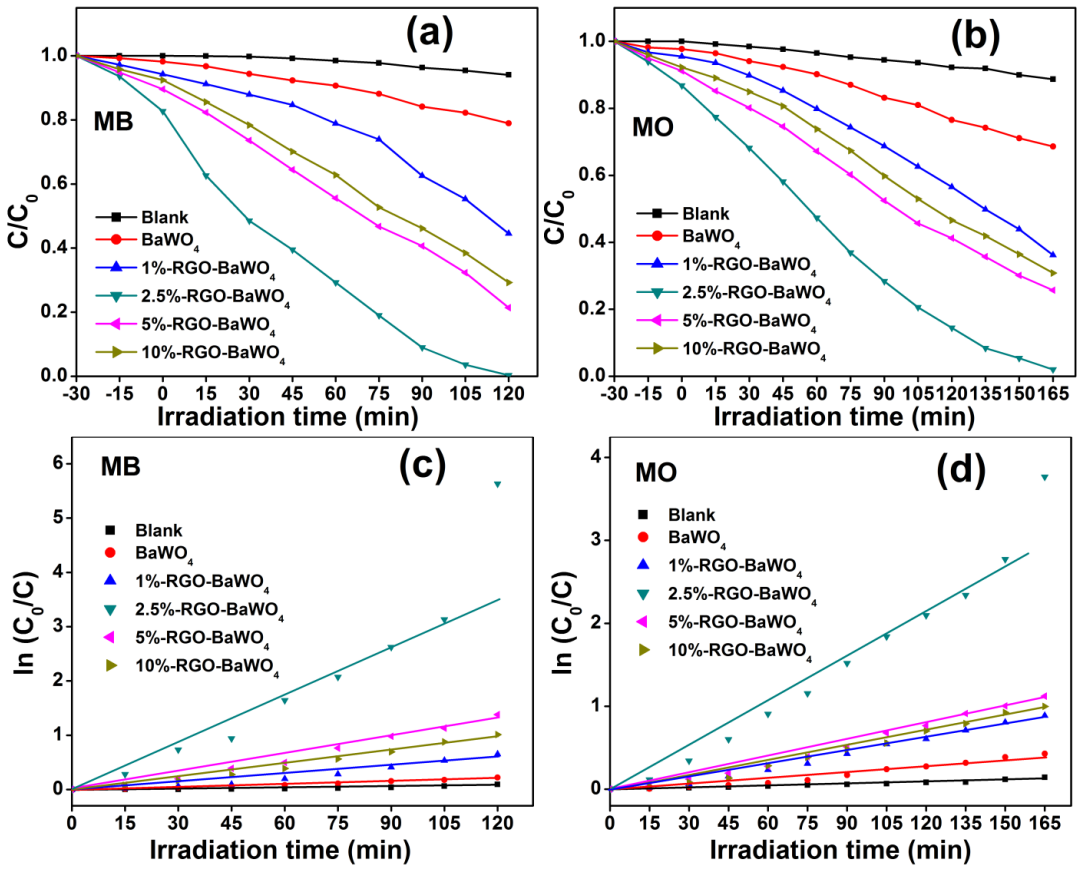

Figure 9. Photocatalytic degradation of (a) MB; (b) MO dye as a function irradiation time; first order kinetic plot of (c) MB and (d) MO dye over different catalysts.

The kinetics of the photocatalytic degradation was studied by the first-order simplification [18] of Langmuir-Hinshelwood (L-H) kinetics, employing equation (3),

$$\ln(C_0/C) = kt \quad (3)$$

where C_0/C is the ratio between the concentration of the dye molecules at adsorption-desorption equilibrium and at irradiation time "t" and "k" is the first-order rate constant (min^{-1}). The "k" value is found from the plot of $\ln(C_0/C)$ versus irradiation time "t" (Figure 9c–d). The efficiency of photodegradation of the RGO-$BaWO_4$ composites increased with increasing the RGO contents from 1 to 10 wt% (Table 1). With increase in the RGO content, initially the efficiency of photocatalytic activity increases up to 2.5%. At 2.5% RGO content, the nanocomposite showed higher efficiency compared to other samples. This may be ascribed to the higher surface area available for charge separation which in turn enhances the catalytic efficiency. The decrease in the activity above 2.5% RGO content may be ascribed to the coverage of RGO on the semiconductor material and hence preventing the latter from effective absorption of incident light radiation and causing low activity [8,22]. This results of surface area analyses of the samples also support this statement.

Table 1. Rate constant values for various catalysts for degradation of MB and MO.

Catalyst	Rate constant k (min^{-1})	
	Methylene Blue	Methyl Orange
$BaWO_4$	0.00182	0.00319
1% RGO-$BaWO_4$	0.00601	0.00664
2.5% RGO-$BaWO_4$	0.03910	0.02092
5% RGO-$BaWO_4$	0.01130	0.00727
10% RGO-$BaWO_4$	0.00927	0.00690

As 2.5 % RGO-$BaWO_4$ exhibited maximum performance, the photocatalytic stability and reusability of this composite are investigated for five consecutive cycles (Table 2). The photocatalytic activity of MB and MO degradation decreased slightly from 99.70 % to 97.68 % and 97.99 % to 89.59 % after five cycles, which indicates that 2.5 % RGO-$BaWO_4$ nanocomposite has excellent reusability. The decreased efficiency may be due to loss of the catalyst during recovery process. Overall, the results indicate that the synthesized composites have excellent recyclability and photocatalytic efficiency.

Table 2. Reusability of the 2.5% RGO-$BaWO_4$ composite in photodegradation of MB and MO dye.

Number of Cycles	Efficiency of degradation (%)	
	Methylene Blue	Methyl Orange
1	99.7	98.0
2	99.0	97.9
3	98.7	94.2
4	98.4	91.7
5	97.7	89.6

3.9. Mechanism of Photocatalytic Activity

The possible photocatalytic mechanisms involved in dye degradation was determined via trapping experiments using the chemicals, 5mM of tertiary butanol (TBA); 5 mM of disodium salt of ethylenediaminetetraaceticacid (EDTA), 5 mM of benzoquinone (BQ) and 10 mM of silver nitrate ($AgNO_3$) to act as scavengers for hydroxyl radicals, holes, superoxide radicals, and electrons respectively during the photocatalytic process [18]. The photodegradation reaction rate showed no much change when TBA was added indicating hydroxyl radicals are not the active species. However, the addition of EDTA, BQ and $AgNO_3$ to the system decreased the efficiency drastically showing that holes and super oxide anion radicals are mainly involved in the photodegradation process (Table 3). As indicated by the results below, a possible schematic scheme for the photocatalytic degradation is given in Figure 10. RGO-$BaWO_4$ composite absorbs the visible light and electron-hole pairs are created in $BaWO_4$. RGO due to its high charge carrier mobility can act as electron acceptor and transporter and delay the recombination of photogenerated electron hole pair. The negatively charged electrons react with dissolved oxygen to produce the superoxide anion radicals ($O_2^{\cdot -}$). The holes react with the water molecules to form hydroxyl radicals ($OH^{\cdot}$).

Table 3. Photocatalytic degradation of MB and MO dye over 2.5% RGO-$BaWO_4$ composites using different scavengers.

Scavenger	Extent of Degradation (%)	
	Methylene Blue	Methyl Orange
None	99.7	98.0
TBA	98.6	94.0
EDTA	73.8	63.0
BQ	54.0	46.9
$AgNO_3$	79.2	70.5

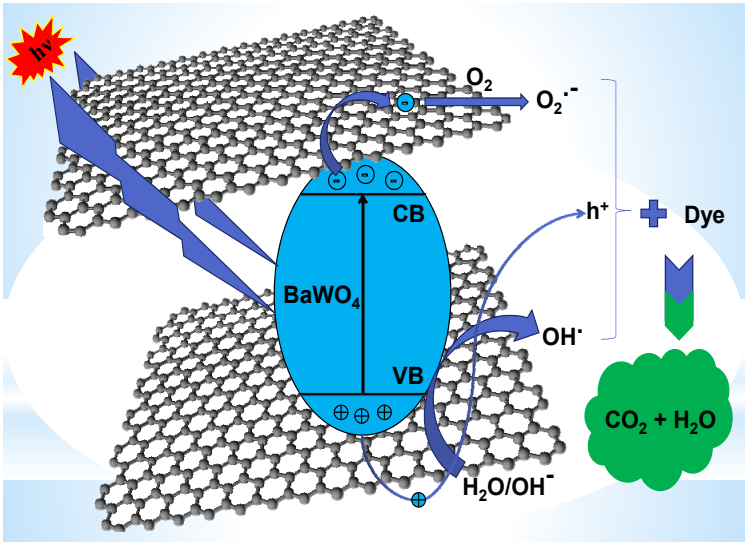

Figure 10. Proposed mechanism for the photocatalytic degradation of dye by RGO-$BaWO_4$ composites.

These active species degrade the dye molecules into products like carbon dioxide and water. The reaction steps are shown in equation 4 to 9.

$$BaWO_4 + h\nu \rightarrow BaWO_4 (e^- + h^+) \quad (4)$$

$$BaWO_4 (e^-) + RGO \rightarrow BaWO_4 + RGO (e^-) \quad (5)$$

$$e^- + O_2 \rightarrow O_2^{\cdot -} \quad (6)$$

$$OH^- + h^+ \rightarrow OH^{\cdot} \quad (7)$$

$$Dye + O_2^{\cdot -} + OH^{\cdot} + h^+ \rightarrow CO_2 + H_2O \quad (8)$$

4. Conclusions

A series of RGO-$BaWO_4$ composites with various compositions have been synthesized via microwave irradiation method. The prepared materials have been characterized by diffraction, microscopic and spectroscopic techniques. The photocatalytic activities of the RGO-$BaWO_4$ composites have been studied using MB and MO dye. The dye degradation efficiency has been determined in the presence of visible light. We observed that the RGO-$BaWO_4$ composites with the optimal RGO content of 2.5 wt% shows the maximum photocatalytic performance of dye degradation in comparison to the other ratios studied. The improved photocatalytic performance of the $BaWO_4$ is due to the increase in visible light absorption range and the reduction in recombination rate of photogenerated electron-hole pair due to the composited RGO. The photocatalytic degradation mechanism involved superoxide anion radical and holes as the active species. The synthesized RGO-$BaWO_4$ had excellent stability and reusability. Hence, the above results indicate that RGO-$BaWO_4$ composite can be a promising eco-friendly photocatalytic material for the treatment of organic dyes.

Acknowledgements

The author M.M.S.J. acknowledges the financial support from the National Institute of Technology Karnataka, Surathkal in the form of research fellowship.

Conflicts of Interest

The authors declare no competing financial interest.

References

1. Sadiq MMJ, Bhat DK (2017) Novel $ZnWO_4$/RGO nanocomposite as high performance photocatalyst. *AIMS Mater Sci* 4: 158–171.
2. Molinari R, Lavorato C, Argurio P (2017) Recent progress of photocatalytic membrane reactors in water treatment and in synthesis of organic compounds. A review. *Catal Today* 281: 144–164.
3. Khan M, Lo IMC (2017) Removal of ionizable aromatic pollutants from contaminated water using nano γ-Fe_2O_3 based magnetic cationic hydrogel: Sorptive performance, magnetic separation and reusability. *J Hazard Mater* 322: 195–204.

4. Liu M, Chen Q, Lu K, et al. (2017) High efficient removal of dyes from aqueous solution through nanofiltration using diethanolamine-modified polyamide thin-film composite membrane. *Sep Purif Technol* 173: 135–143.
5. Bilal M, Asgher M, Saldivar RP, et al. (2017) Immobilized ligninolytic enzymes: An innovative and environmental responsive technology to tackle dye-based industrial pollutants—A review. *Sci Total Environ* 576: 646–659.
6. Taufik A, Saleh R (2017) Synthesis of iron (II, III) oxide/zinc oxide/copper (II) oxide (Fe_3O_4/ZnO/CuO) nanocomposites and their photosonocatalytic property for organic dye removal. *J Colloid Interf Sci* 491: 27–36.
7. Chen D, Zhu H, Yang S, et al. (2016) Micro-nanocomposites in environmental management. *Adv Mater* 28: 10443–10458.
8. Banerjee S, Pillai SC, Falaras P, et al. (2014) New insights into the mechanism of visible light photocatalysis. *J Phys Chem Lett* 5: 2543–2554.
9. Teoh WY, Scott JA, Amal R (2012) Progress in heterogeneous photocatalysis: From classical radical chemistry to engineering nanomaterials and solar reactors. *J Phys Chem Lett* 3: 629–639.
10. Li C, Xu Y, Tu W, et al. (2017) Metal-free photocatalysts for various applications in energy conversion and environmental purification. *Green Chem* 19: 882–899.
11. Selvakumar M, Bhat DK (2012) Microwave synthesized nanostructured TiO_2-activated carbon composite electrodes for supercapacitor. *Appl Surf Sci* 263: 236–241.
12. Bhat DK (2008) Facile synthesis of ZnO nanorods by microwave irradiation of zinc-hydrazine hydrate complex. *Nanoscale Res Lett* 3: 31–35.
13. Bhatt AS, Bhat DK (2012) Crystallinity, magnetic and electrochemical studies of PVDF/Co_3O_4 polymer electrolyte. *Mater Sci Eng B* 177: 127–131.
14. Bhatt AS, Bhat DK (2012) Influence of nanoscale NiO on magnetic and electrochemical behavior of PVDF based polymer nanocomposites. *Polym Bull* 68: 253–261.
15. Paola AD, Lopez EG, Marci G, et al. (2012) A survey of photocatalytic materials for environmental remediation. *J Hazard Mater* 211–212: 3–29.
16. Bhatt AS, Bhat DK (2011) Crystallinity, conductivity and magnetic properties of PVDF-Fe_3O_4 composite films. *J Appl Polym Sci* 119: 968–972.
17. Hisatomi T, Kubota J, Domen K (2014) Recent advances in semiconductors for photocatalytic and photoelectrochemical water splitting. *Chem Soc Rev* 43: 7520–7535.
18. Sadiq MMJ, Shenoy US, Bhat DK (2016) Novel RGO-$ZnWO_4$-Fe_3O_4 nanocomposite as high performance visible light photocatalyst. *RSC Adv* 6: 61821–61829.
19. Sadiq MMJ, Bhat DK (2016) Novel RGO-$ZnWO_4$-Fe_3O_4 nanocomposite as an efficient catalyst for rapid reduction of 4-nitrophenol to 4-aminophenol. *Ind Eng Chem Res* 55: 7267–7272.
20. Sadiq MMJ, Nesaraj AS (2014) Soft chemical synthesis and characterization of $BaWO_4$ nanoparticles for photocatalytic removal of Rhodamine B present in water sample. *J Nanostruct Chem* 5: 45–54.
21. Sudhakar YN, Selvakumar M, Bhat DK, et al. (2014) Reduced graphene oxide derived from used cell graphite, and its green fabrication as eco-friendly supercapacitor. *RSC Adv* 4: 60039–60051.
22. Zhang N, Yang MQ, Liu S, et al. (2015) Waltzing with the versatile platform of graphene to synthesize composite photocatalysts. *Chem Rev* 115: 10307–10377.
23. Subramanya B, Bhat DK (2015) Novel eco-friendly synthesis of graphene directly from graphite using TEMPO and study of its electrochemical properties. *J Power Sources* 275: 90–98.

24. Li X, Yu J, Wageh S (2016) Graphene in photocatalysis: A review. *Small* 12: 6640–6696.
25. Subramanya B, Bhat DK, Shenoy SU, et al. (2015) Novel Fe-Ni-Graphene composite electrode for hydrogen production. *Int J Hydrogen Energ* 40: 10453–10462.
26. Subramanya B, Ullal Y, Shenoy SU, et al. (2015) Novel Co-Ni-Graphene composite electrodes for hydrogen production. *RSC Adv* 5: 47398–47407.
27. Hummers Jr WS, Offeman RE (1958) Preparation of graphitic oxide. *J Am Chem Soc* 80: 1339–1339.
28. Subramanya B, Bhat DK (2015) Novel one-pot green synthesis of graphene in aqueous medium under microwave irradiation using regenerative catalyst and study of its electrochemical properties. *New J Chem* 39: 420–430.
29. Szabo T, Berkesi O, Forgo P, et al. (2006) Evolution of surface functional groups in a series of progressively oxidized graphite oxides. *Chem Mater* 18: 2740–2749.
30. Cavalcante L, Sczancoski J, Lima Jr L, et al. (2008) Synthesis, characterization, anisotropic growth and photoluminescence of $BaWO_4$. *Cryst Growth Des* 9: 1002–1012.

AIMS Press